

Empirical $spds^*$ tight-binding calculation for cubic semiconductors: General method and material parameters

Jean-Marc Jancu, Reinhart Scholz,^{*} Fabio Beltram, and Franco Bassani

Scuola Normale Superiore and Istituto Nazionale per la Fisica della Materia, Piazza dei Cavalieri 7, I-56126 Pisa, Italy

(Received 17 July 1997)

An empirical tight-binding method for tetrahedrally coordinated cubic materials is presented and applied to group-IV and III-V semiconductors. The present $spds^*$ method extends existing calculations by the inclusion of all five d orbitals per atom in the basis set. On-site energies and two-center integrals between nearest neighbors in the Hamiltonian are fitted to measured energies, pseudopotential results, and the free-electron band structure. We demonstrate excellent agreement with pseudopotential calculations up to about 6 eV above the valence-band maximum even without inclusion of interactions with more distant atoms and three-center integrals. The symmetry character of the Bloch functions at the X point is considerably improved by the inclusion of d orbitals. Density of states, reduced masses, and deformation potentials are correctly reproduced. [S0163-1829(98)01011-X]

I. INTRODUCTION

Over the last decades, the tight-binding (TB) method has received considerable attention, both because of its intuitive simplicity and its realistic description of structural and dielectric properties in terms of chemical bonds.^{1–5} Since the approach uses small sets of basis functions, the computational effort is smaller than that required by methods based on plane waves. Therefore, it allows one to consider large systems (e.g., structured interfaces, molecular clusters, mesoscopic structures) with unit cells containing hundreds of atoms, where plane-wave methods come to the limits of applicability with present computers. The Slater-Koster suggestion¹ to treat the TB approach as an interpolation scheme was extensively used in a wide range of compounds from transition metals to semiconductor crystals. Within a minimal sp^3 basis and interactions only between nearest-neighbor atoms, the empirical Slater-Koster model can describe the valence-band energy dispersion satisfactorily,^{2,3} but fails to reproduce the indirect gap of semiconductors correctly, especially at the X point. Conduction bands of group-IV and -III-V compounds, however, were extensively and successfully analyzed with pseudopotential methods.^{6–12} These studies showed that the lowest conduction state at X is not entirely antibonding, contrary to a TB description in a minimal basis.³ As a direct consequence, an erroneous positive pressure coefficient of the gap $\Gamma_{8v} \rightarrow X_{6c}$ is calculated within an sp^3 model. Richardson and co-workers^{9,10} showed that the free-electron character of the charge densities at the Γ , X , and L points is monitored by contributions of d symmetry, stemming from unoccupied atomic d orbitals. Γ_{6c} and L_{6c} states have a similar electronic charge density concentrated near the atoms, but, at the L point, symmetry imposes a small d component. At X_{6c} , the d contribution is even larger,^{9,12} but contrary to L_{6c} and Γ_{6c} , the charge distribution is very delocalized.¹⁰

To mimic the influence of the excited d states, Vogl, Hjalmarson, and Dow added an s^* orbital to the sp^3 basis, and achieved the correct positions of the lowest conduction

minima at X and L .⁴ However, transverse masses at these points and the second conduction band are in poor agreement with experiment,¹³ so that the sp^3s^* TB model is only of limited value for the calculation of optical properties involving points at the surface of the Brillouin zone.

Following the recognition of the importance of d states in pseudopotential calculations,⁹ the inclusion of d -excited states of the $e_1(\Gamma_3)$ representation of T_d in a TB basis was attempted, leading to the development of an sp^3d^2 TB model.¹³ While several band properties are better described than in a minimal basis, this approach turns out to be insufficient because the $t_2(\Gamma_4)$ -like d orbitals are of crucial importance both for the Γ_4 states at Γ and for the lowest conduction band at L and X . In both types of TB models, the evaluation of spectral functions turns out to be troublesome because all different angular momentum components of the Bloch functions would be required for quantitative agreement.^{13,14}

From the comparison of pseudopotential calculations with these existing TB models, the necessity to include the full d symmetry near the X point is obvious,¹² so that it seems a natural issue to develop a TB model based on the ten atomiclike orbitals ($s; x, y, z; xy, yz, xz, x^2 - y^2, 3z^2 - r^2; s^*$) per atom, corresponding to an $sp^3d^5s^*$ basis. As will be demonstrated in this paper in some detail, most of the deficiencies of smaller TB models can be overcome. In fact, this approach can be regarded as the simplest Hamiltonian reproducing the main features of the valence band and the two lowest conduction bands.

While TB methods based on extended atomic wave functions depend on overlap matrices, Wannier functions of the corresponding symmetries are orthogonal on different atomic sites. Actually, the calculation of such Wannier functions was performed only in special cases,¹⁵ but we shall take their existence for granted without attempting their calculation. Instead, we characterize them by their on-site energies and the two-center energy integrals between adjacent sites, the nondiagonal overlap elements being zero. We shall show in the following that accurate results can be obtained even without consideration of two-center energy integrals between more distant atoms and of three-center integrals.

In Sec. II, we review elementary group theoretical arguments^{16,17} and relate them to the free-electron band structure and the atomic symmetries of our basis set. With the construction of symmetry-adapted Bloch functions, a block-diagonal TB Hamiltonian can be obtained.^{18,19} In Sec. III, this block structure is used for the calculation of the TB parameters of the empty lattice. Based on these starting values, we present our numerically determined TB parameters in Sec. IV, together with the resulting band structures for group-IV semiconductors and III-V compounds. Some of the ordering problems of consecutive conduction extrema at L and X are resolved. In Sec. V we investigate uniaxial and hydrostatic deformation potentials as a function of the distance dependence of the TB parameters. All deficiencies of former TB models are resolved, e.g., the erroneous sign of the X_{6c} deformation potential. In Sec. VI, we summarize the improvements obtained and outline some possible extensions.

II. SYMMETRY ANALYSIS

A. Free-electron band structure

Before addressing details of the TB Hamiltonian, it is useful to recall the free-electron band structure. It is derived from the potential-free Hamiltonian

$$H = \frac{\mathbf{p}^2}{2m_0}, \quad (1)$$

where m_0 is the free-electron mass. The translational symmetry of the crystal leads to parabolic free-electron bands,

$$E_{\mathbf{G}}(\mathbf{k}) = \frac{(\mathbf{k} + \mathbf{G})^2}{2m_0}, \quad (2)$$

where the wave vector \mathbf{k} is confined within the first Brillouin zone, and \mathbf{G} is a vector of the reciprocal lattice. At the Γ point, the lowest energies derive from the shortest vectors of the reciprocal lattice: $\mathbf{G} = (0,0,0)$, $K\langle 1,1,1 \rangle$, and $K\langle 2,0,0 \rangle$, where $K = 2\pi/a$ is the unit length in reciprocal space and $\langle \dots \rangle$'s denote sets of degenerate wave vectors. Energies at high symmetry points of the Brillouin zone can then be expressed in units of $E_{\langle 1,0,0 \rangle} = \hbar^2 K^2 / 2m_0$, e.g., $E_{\Gamma} = 0, 3, 4, 8, \dots$, and $E_X = 1, 2, 5, 6, \dots$. The energy unit $E_{\langle 1,0,0 \rangle}$ will be omitted in the following when discussing the free-electron band structure.

B. Representations of T_d and its subgroups

The following arguments will be based on the representations of the tetrahedral group T_d , but the generalization to the octahedral group O_h is straightforward. In order to use a unified notation throughout, we shall also use representations of T_d for the free electrons, where in principle the larger group O_h applies. For the representations we shall use the conventions of Dresselhaus²⁰ (for correspondence with other notations see, e.g., Ref. 21).

Γ is the point of highest symmetry in the Brillouin zone, therefore the full tetrahedral point group applies. The compatibilities between the atomic symmetries and the representations of T_d are¹⁷

$$\begin{aligned} s, s^* &\rightarrow \Gamma_1, \\ p &\rightarrow \Gamma_4, \\ d &\rightarrow \Gamma_3 + \Gamma_4. \end{aligned} \quad (3)$$

Obviously, two representations for d states occur, and the corresponding states will be labeled $d(\Gamma_3)$ and $d(\Gamma_4)$ in the following. Using standard textbook results, irreducible decompositions of sets of reciprocal-lattice vectors can be obtained:^{17,21}

$$\begin{aligned} (0,0,0) &\rightarrow \Gamma_1, \\ \langle 1,1,1 \rangle &\rightarrow 2\Gamma_1 + 2\Gamma_4, \\ \langle 2,0,0 \rangle &\rightarrow \Gamma_1 + \Gamma_3 + \Gamma_4. \end{aligned} \quad (4)$$

As the Hamiltonian has the highest possible symmetry Γ_1 , only bands of the same irreducible representations interact. The decomposition of the 20×20 $spds^*$ TB Hamiltonian yields the following submatrices for the different representations: 4×4 for Γ_1 , two identical 2×2 blocks for Γ_3 , and three times a 4×4 block for Γ_4 . From the compatibilities of the atomic symmetries and the representations of the tetrahedral group it can be derived that the Γ_1 block is composed of two s and two s^* orbitals, and each of the Γ_3 blocks of two $d(\Gamma_3)$ orbitals. The three Γ_4 submatrices contain each two p and two $d(\Gamma_4)$ states, e.g., x_a, x_c, yz_a , and yz_c , and cyclic permutations of Cartesian directions.

For the purposes of our TB model, it is instructive to investigate the compatibilities with the representations of the subgroup C_{2v} along the Δ line between Γ and X :^{20,21}

$$\begin{aligned} \Gamma_1 &\rightarrow \Delta_1, \\ \Gamma_3 &\rightarrow \Delta_1 + \Delta_2, \\ \Gamma_4 &\rightarrow \Delta_1 + (\Delta_3 + \Delta_4). \end{aligned} \quad (5)$$

Comparing these compatibilities and the decomposition of the TB Hamiltonian at Γ , we arrive at subblocks of dimension 10×10 for Δ_1 , 2×2 for Δ_2 , and 4×4 for Δ_3 and Δ_4 . The latter two contain equivalent matrix elements because they are degenerate. The small submatrices for Δ_2 and Δ_3 will be exploited below for the assignment of the parameters involved.

C. TB basis required for numerical completeness

A complete basis for the highest occupied states in isolated atoms consists of valence shell s and p states only. Because the interaction matrix elements between orbitals of adjacent sites in the solid are not much smaller than the spacing of the atomic energy levels, one cannot expect that this basis remains close to complete for the valence bands. Instead, for each representation Γ_i with occupied valence states, *at least* a second type of basis orbital is required for a better approximation to completeness. Comparing with the decomposition of the sets of shortest reciprocal-lattice vectors at Γ , the following bases are the natural choice:

$$\begin{aligned}\Gamma_1 &: \{s, s^*\}, \\ \Gamma_4 &: \{p, d\}.\end{aligned}\quad (6)$$

Using instead an *effective s* orbital and no *s** orbital for the Γ_1 basis, a good description of the band structure remains possible, but the correspondence with atomic wave functions and the transferability between different bulks are lost. Furthermore, important features like the anion-cation character of Γ_1 wave functions give erroneous results in this smaller basis; compare the discussion in Sec. IV.

III. MODEL SEMICONDUCTOR: FREE ELECTRONS

Before coming to real materials, we derive the interaction parameters of the empty-lattice model by requiring consistency between the TB bands and the free-electron energy spectrum. For this purpose, we use the submatrices of the Hamiltonian identified in Sec. II. Coupling matrices will be given below in the general form for polar materials, but the free-electron TB parameters will be discussed in the nonpolar case.

The energy zero will be taken at (0,0,0), and the energy unit $E_{\langle 1,0,0 \rangle}$ will not be given explicitly. For the interaction parameters, we shall use the convention of Slater and Koster¹ for the bare two-center parameters, e.g., $ss\sigma$, while the Hamiltonian matrix elements between basis states are denoted with V , e.g., $V_{ss\sigma}=4 ss\sigma$.

A. Subgroup C_{2v} : representations Δ_2 and Δ_3

As discussed in Sec. II, the Δ line gives the most instructive block diagonalization. The submatrix for Δ_2 reads

$$H(\Delta_2) = \begin{pmatrix} E_d^a & V_{dd}(\Delta_2) \\ V_{dd}(\Delta_2) & E_d^c \end{pmatrix}, \quad (7)$$

where

$$V_{dd}(\Delta_2) = \frac{4}{3}(2 dd\pi + dd\delta) \cos \frac{ka}{4}. \quad (8)$$

The angular argument $ka/4$ runs between zero at Γ and $\pi/2$ at the X point, with $k=k_X=2\pi/a$. The comparison with the analysis in Sec. II demonstrates that the two Δ_2 bands shall pass through $\langle 1,2,0 \rangle$ at X and $\langle 2,0,0 \rangle$ and $\langle 2,2,0 \rangle$ at Γ . First of all, this determines the on-site d -energy of the nonpolar empty lattice, $E_d^a=E_d^c=E_d$. It can be determined at the X point, where the off-diagonal matrix elements of Eq. (7) vanish:

$$E_d = E_{\langle 1,2,0 \rangle} = 5. \quad (9)$$

The asymmetric splitting of the Δ_2 bands cannot be obtained in our simple nearest-neighbor overlap-free TB model. Nevertheless, the analysis of the lower band allows the assignment of the parameter $V_{dd}(\Delta_2)$:

$$V_{dd}(\Delta_2, k=0) = \frac{4}{3}(2 dd\pi + dd\delta) = E_{\langle 1,2,0 \rangle} - E_{\langle 2,0,0 \rangle} = 1, \quad (10)$$

where $dd\pi \geq -dd\delta > 0$ (Ref. 3) was used to set the sign of $V_{dd}(\Delta_2, k=0)$. As usual in overlap-free TB models, the

highest band included is not described correctly, but this upper limit of applicability of the parameters is now pushed to about $E=6$ and 3 energy units from the point $\langle 1,1,1 \rangle$ governing the surroundings of the direct gap in real materials. The submatrix for the Δ_3 bands reads

$$H(\Delta_3) = \begin{pmatrix} E_p^a & V_{pp}(\Delta_3) & 0 & V_{pd}^{ac}(\Delta_3) \\ V_{pp}^*(\Delta_3) & E_p^c & V_{pd}^{ca}(\Delta_3) & 0 \\ 0 & V_{pd}^{ca*}(\Delta_3) & E_d^a & V_{dd}(\Delta_3) \\ V_{pd}^{ac*}(\Delta_3) & 0 & V_{dd}^*(\Delta_3) & E_d^c \end{pmatrix}, \quad (11)$$

where the various abbreviations are explained in the Appendix. Equation (11) allows us to estimate the on-site p energies $E_p=E_p^a=E_p^c$ in the empty-lattice model, because the sum over the four Δ_3 bands described by $H(\Delta_3)$ is equal everywhere to the trace $\text{Tr}[H(\Delta_3)] = 2E_p + 2E_d$. For free electrons, the sum over the four lowest bands of this symmetry varies between 18 at Γ and X and 17 at the midpoint between them. This shows that our model cannot agree with the k dependence of this sum without additional overlap matrix elements or interactions between more distant atoms. In order to have the correct value at the high-symmetry points, we take $2E_p + 2E_d = 18$, or

$$E_p = 4. \quad (12)$$

The two-center matrix elements of Eq. (11) are deduced for a diamond structure by equaling pairs of interaction parameters, e.g., $p_a d_c \sigma = p_c d_a \sigma = p d \sigma$. For the free-electron spectra, the energetic positions of the four lowest Δ_3 bands at X are $E_X = 2, 5, 5$, and 6. Since the highest valence band at X is known to have nearly 100% p character in real semiconductors,¹² we assume that p and d bands decouple at this point, so that $E_X = 2$ and 6 arise from p states alone, and $E_X = 5$ and 5 from d states. Because the energetic positions of the latter coincide with E_d , we deduce that d states do not interact with each other. Therefore, we arrive at the following assignment of coupling parameters:

$$V_{dd}(\Delta_3, k=k_X) = 0, \quad (13)$$

$$V_{pd}(\Delta_3, k=k_X) = 0, \quad (14)$$

$$|V_{pp}(\Delta_3, k=k_X)| = 2 \Rightarrow V_{xy} = 2. \quad (15)$$

The two equations (10) and (13) are not sufficient to determine the three two-center integrals among d states, $dd\sigma$, $dd\pi$, and $dd\delta$. The third restriction is found by *assuming* that the bonding d state at Γ shall pass through $E=4$. This energetic position occurs in the free-electron band structure, but it will be changed later by the inclusion of the p - d interaction at Γ . From the assumed position of the bonding d state at Γ , we obtain a third equation for the interactions between d states,

$$V_{dd}(\Gamma_4) = V_{dd}(\Delta_3, k=0) = -1, \quad (16)$$

which is found from considering only the d submatrix in Eq. (11). Equations (10), (13), and (16) yield the two-center integrals among d states:

$$dd\sigma = -\frac{1}{4}, \quad (17)$$

$$dd\pi = \frac{3}{4}, \quad (18)$$

$$dd\delta = -\frac{3}{4}. \quad (19)$$

Equation (14) gives the ratio of $pd\sigma$ and $pd\pi$:

$$pd\pi = -\sqrt{3}pd\sigma. \quad (20)$$

In the free-electron spectra, the two lowest bands arising from the Δ_3 symmetry are degenerate at Γ with the eigenvalue $E(\Gamma_4)=3$. This gives two restrictions for the p - p and p - d interactions:

$$V_{pp}(\Delta_3, k=0) = V_{xx} = -\frac{1}{2}, \quad (21)$$

$$|V_{pd}(\Delta_3, k=0)| = |V_{pd}(\Gamma_4)| = \frac{\sqrt{6}}{2}. \quad (22)$$

Solving Eqs. (15) and (21) for the p - p interactions, and Eqs. (14) and (22) for the p - d interactions, we obtain

$$pp\sigma = \frac{7}{8}, \quad (23)$$

$$pp\pi = -\frac{5}{8}, \quad (24)$$

$$pd\sigma = -\frac{\sqrt{6}}{8}, \quad (25)$$

$$pd\pi = \frac{3\sqrt{2}}{8}. \quad (26)$$

This demonstrates that the analysis of the Δ_3 bands in their limits at Γ and X fully determines the on-site p and d energies and their two-center integrals for a free electron. In real materials, the interaction parameters are modified by the atomic pseudopotentials, lifting some of the degeneracies, e.g., of the two energetic positions $E(\Gamma_4)=3$.

B. Γ_1 representation: interactions among s , s^*

The Γ point is most instructive for calculating the interaction parameters among s and s^* states, because they determine the Γ_1 coupling matrix

$$H(\Gamma_1) = \begin{pmatrix} E_s^a & V_{ss\sigma} & 0 & V_{ss^*\sigma}^{ac} \\ V_{ss\sigma} & E_s^c & V_{ss^*\sigma}^{ca} & 0 \\ 0 & V_{ss^*\sigma}^{ca} & E_{s^*}^a & V_{s^*s^*\sigma} \\ V_{ss^*\sigma}^{ac} & 0 & V_{s^*s^*\sigma} & E_{s^*}^c \end{pmatrix}, \quad (27)$$

where $V_{ss\sigma}=4 ss\sigma$, etc. In the free-electron spectra, the lowest energies of this symmetry are $E(\Gamma_1)=0, 3, 3$, and 4 , but the highest of them is related to the next s shell not included in our basis, so that only the lower three can be used for assigning the coupling and on-site parameters. One of the Δ_1 bands starting at $E(\Gamma_1)=3$ shall end at $E_X=6$. Assuming that the s^* state is only weakly coupled to p and d states, we set the corresponding interactions $s^*p\sigma$ and

$s^*d\sigma$ to zero. All interactions among s^* and s states vanish at X by symmetry, so that $E_X=6$ can be used to assign

$$E_{s^*} = 6. \quad (28)$$

For E_s , the only restriction we can derive is $2E_s > 3$, which corresponds to the sum of the lowest two Γ_1 energies. A good choice turns out to be

$$E_s = 2. \quad (29)$$

The two-center integrals are then derived from the three lowest Γ_1 energies. With the usual phase convention,³ we obtain

$$ss\sigma = -\frac{5}{16}, \quad (30)$$

$$s^*s^*\sigma = -\frac{15}{16}, \quad (31)$$

$$ss^*\sigma = -\sqrt{27}/16. \quad (32)$$

C. Interactions between $\{s, s^*\}$ and $\{p, d\}$

The four undetermined matrix elements of the free-electron Hamiltonian concern the interaction of the s and s^* states with p and d . The smaller two, $s^*p\sigma$ and $s^*d\sigma$, have already been assumed to vanish. For the other two, we fix the ratio $sp\sigma/sd\sigma = -\frac{3}{2}$, so that only one matrix element remains to be determined. We derive it from the lowest energy of the Δ_1 bands at X , $E_X=1$, yielding

$$sp\sigma = 0.6468, \quad (33)$$

$$sd\sigma = -0.4312. \quad (34)$$

D. Resulting free-electron band structure

The parameters derived above are given in Table I. In Fig. 1, we illustrate the influence of the various interaction parameters on the free-electron band structure, and in the upper row, subsets of the atomic symmetries $\{s, s^*\}$, p , and d are shown separately. The $\{s, s^*\}$ bands in Fig. 1(a) give only the correct positions of the Γ_1 states, while at all other points of the Brillouin zone, they are coupled into larger submatrices influenced by p and d . For our special choice $s^*p\sigma = s^*d\sigma = 0$, the only exception is the correct position $E_X = 6$. The twice degenerate p bands in Fig. 1(b) decouple at X for the p - d parameters we use, but this feature depends on the parameter choice, so that, generally speaking, the p bands have nowhere a point where they remain uncoupled to the states of s and d symmetry. Nevertheless, the highest valence band will present wave functions with a dominant p contribution. In fact, the lower Λ_3 and Δ_3 bands obtained from p states alone are already close to the final band positions. The d bands in Fig. 1(c) determine the Δ_2 bands, and the lower one $\langle 0,2,0 \rangle \rightarrow \langle 1,2,0 \rangle$ approximately reproduces the free-electron band. A remarkable feature of the d bands is the very low bonding state at X . Its bonding character will be of crucial importance for the deformation potential of the conduction-band minimum at X (see Secs. IV and V below). The splitting of the d bands at X can be shown to be

$$(\Delta E_d)_X = \frac{8\sqrt{3}}{9} (dd\pi - dd\delta), \quad (35)$$

which is equal to $4\sqrt{3}/3 = 2.3$ for our model parameters. The symmetry character of the corresponding wave function of

TABLE I. Free-electron parameters in units of $E_{\langle 1,0,0 \rangle}$. First column: analytically derived values; second column: fitted values. The third column shows universal parameters of the *sp* model (Ref. 22) for comparison.

	Analytic	Fitted	<i>sp</i> model (Ref. 22)
E_s	2.0	1.9378	1.5
E_p	4.0	3.9491	3.5
E_d	5.0	4.9823	
E_{s^*}	6.0	6.0733	
$ss\sigma$	$-\frac{5}{16} = -0.3125$	-0.3214	$-\frac{3}{8} = -0.375$
$s^*s^*\sigma$	$-15/16 = -0.9375$	-0.9317	
$ss^*\sigma$	$-\sqrt{27}/16 = -0.3248$	-0.3093	
$sp\sigma$	0.6468	0.5836	$\sqrt{15}/8 = 0.4841$
$s^*p\sigma$	0	0.2199	
$sd\sigma$	-0.4312	-0.3837	
$s^*d\sigma$	0	-0.0198	
$pp\sigma$	$\frac{7}{8} = 0.875$	0.8526	$\frac{7}{8} = 0.875$
$pp\pi$	$-\frac{5}{8} = -0.625$	-0.5977	$-\frac{1}{4} = -0.25$
$pd\sigma$	$-\sqrt{6}/8 = -0.3062$	-0.1849	
$pd\pi$	$3\sqrt{2}/8 = 0.5303$	0.6230	
$dd\sigma$	$-\frac{1}{4} = -0.25$	-0.2311	
$dd\pi$	$\frac{3}{4} = 0.75$	0.7309	
$dd\delta$	$-\frac{3}{4} = -0.75$	-0.7248	

this lowest *d* state at *X* is half $d(\Gamma_3)$ (e_1) and half $d(\Gamma_4)$ (t_2). Except for $V_{s^*s^*\sigma} = -\frac{15}{4}$ derived from Eq. (31), Eq. (35) gives the largest interaction parameter of our TB model at any of the high-symmetry points Γ , *L*, and *X*. Obviously, such an extremely large interaction matrix element cannot be derived in a perturbative approach, so that the analysis of the free-electron bands is required for an estimate of its magnitude.

In Fig. 1(d) we show the bands determined by the subset $\{p,d\}$. In addition to the Δ_2 bands already given by *d* states alone, this subset determines entirely the double degenerate-bands of Δ_3 and Δ_3 symmetry. At Γ , the lower two coincide with the required energy $E(\Gamma_4) = 3$, but the upper two occur at $E(\Gamma_4) = 5.5$ and 6.5 instead of $E(\Gamma_4) = 4.8$. These deviations are due to the inherent limitations of our nearest-neighbor TB model mentioned above, and the requirements for the *X* point on the analytic determination of parameters. For real materials, the error for the third Γ_4 -position will be smaller by a factor of about $\frac{1}{3}$.

In Fig. 1(e), we show the complete band structure according to the above parameters; compare Table I. The overall agreement with the free-electron band structure [shown by the thin lines in Fig. 1(e)] is good. Nevertheless, there remain

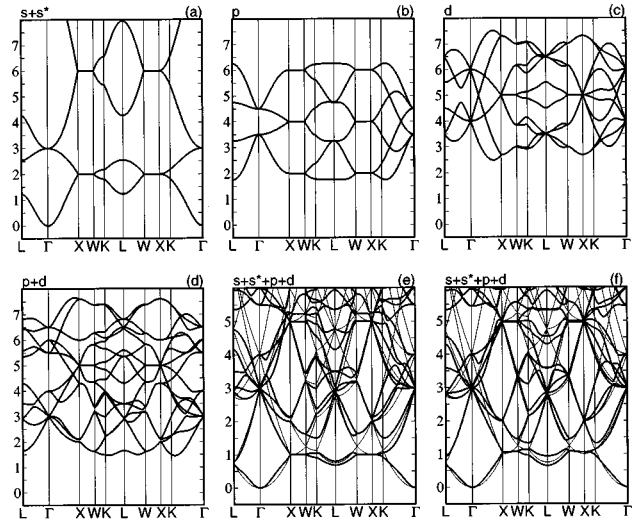


FIG. 1. Empirical TB band structure approaching the free-electron bands. (a)–(e) calculated with the analytically derived parameters in Table I: (a) $\{s, s^*\}$ only, without interactions with the other symmetries; (b) same for *p*; (c) same for *d*; (d) including all interactions within the $\{p, d\}$ subset; (e) with all interactions (thick lines) and free-electron bands superimposed (thin lines). (f) Bands with the parameters in Table I obtained from the numerical fit (thick lines), with free-electron bands superimposed (thin lines). The energy unit is $E_{\langle 1,0,0 \rangle} = \hbar^2 K^2 / 2m_0$ (see Sec. II A).

some significant discrepancies, as can be seen in the regions around $E_L = 2.75$ and $E_W = 3.25$.

In order to improve the free-electron band structure, we optimized the TB parameters by a conjugate gradient scheme. The resulting parameters are given in Table I, and the corresponding bands are shown in Fig. 1(f). The agreement with the superimposed free-electron band structure is improved, in particular for the solution of the discrepancies mentioned above around $E_L = 2.75$ and $E_W = 3.25$. The main residual deficiencies up to $E = 5$ are a missing s^{**} band starting at $\langle 2,0,0 \rangle$, the third Δ_3 band which remains much too high near Γ , and the somewhat low values of the bands at *L* which should pass through $E_L = 4.75$.

Comparing the fitted values with the analytically derived parameters in Table I, one finds generally good agreement with a few exceptions. From the two preset values $s^*p\sigma = s^*d\sigma = 0$, only the former suffers a large change, while the latter remains very small. A further significant change occurs for $pd\sigma$ and $pd\pi$, which is responsible for the better agreement near $E_W = 3.25$.

The parameters in the *sp* model according to Froyen and Harrison are given in Table I for comparison.²² Some of the old features are reproduced in our model, like, e.g., $E_p - E_s = 2$, and in general parameters are similar, except for $pp\pi$. The shift of the on-site energies E_p and E_s by 0.5 upwards in the larger *spds** basis can be understood from the fact that the valence bands are pushed down by additional interactions with the higher-lying states *d* and s^* , resulting in the same valence-band positions as in the *sp* model. The strongly different values for $pp\pi$ are related to the required Δ_3 bands at Γ and *X*: the *sp* model results in $E(\Gamma_4) = 3$ and 4 and $E(X_5) = 2$ and 5, while we try to reproduce both Γ_4 -like bands at $E(\Gamma_4) = 3$. The *sp* model reproduces only half of

TABLE II. Empirical TB parameters for group-IV semiconductors. The lattice constant a and energy unit $E_{\langle 1,0,0 \rangle}$ are given at room temperature (Ref. 27); all other parameters are intended to be low-temperature values, in units of eV, with the energy zero at the valence maximum.

	C	Si	Ge
$a(\text{\AA})$	3.5668	5.430	5.6563
$E_{\langle 1,0,0 \rangle}$	11.823	5.1016	4.7014
E_s	-1.0458	-2.0196	-3.2967
E_p	7.0850	4.5448	4.6560
E_d	27.9267	14.1836	13.0143
E_{s^*}	38.2661	19.6748	19.1725
$ss\sigma$	-4.3882	-1.9413	-1.5003
$s^*s^*\sigma$	-2.6737	-3.3081	-3.6029
$s^*s\sigma$	-2.3899	-1.6933	-1.9206
$sp\sigma$	5.4951	2.7836	2.7986
$s^*p\sigma$	5.1709	2.8428	2.8177
$sd\sigma$	-2.7655	-2.7998	-2.8028
$s^*d\sigma$	-2.3034	-0.7003	-0.6209
$pp\sigma$	7.5480	4.1068	4.2541
$pp\pi$	-2.6363	-1.5934	-1.6510
$pd\sigma$	-2.1621	-2.1073	-2.2138
$pd\pi$	3.9281	1.9977	1.9001
$dd\sigma$	-4.1813	-1.2327	-1.2172
$dd\pi$	4.9779	2.5145	2.5054
$dd\delta$	-3.9884	-2.4734	-2.1389
$\Delta/3$	0.0	0.0195	0.1325

the Γ_1 and Γ_4 bands resulting from $\langle 1,1,1 \rangle$, but the corresponding interaction parameter $pp\pi = -\frac{1}{4}$ is quite realistic for real materials; see below.

The TB parameters of the empty d shell demonstrate that extended d -wave functions cannot coincide with those of deep d orbitals. As a direct consequence, our results are in contrast to earlier estimates for metal d bands.²³ For the interactions among d states, the most striking feature is that $dd\sigma$ is the smallest of the three two-center integrals: The ratio given by Harrison was $dd\sigma:dd\pi:dd\delta = -6:4:-1$,²³ while our result is $-1:3:-3$. For the interactions between p and d , the ratio $-pd\pi/pd\sigma = 3.37$ is extremely large, contrary to transition-metal compounds, where $-pd\pi/pd\sigma \lesssim 1$ would be expected.²³ As we will show below, the large ratio above never occurs in real semiconductors: It is only required for good agreement with the free-electron bands.

IV. MATERIAL PARAMETERS AND BAND STRUCTURES FOR GROUP-IV AND III-V SEMICONDUCTORS

A. Parameters and band structures

The starting values of the TB parameters for real materials are derived from the free-electron results in Table I, and atomic energies. In a second step, the deviation of the result-

ing band energies from various reference values is minimized numerically.²⁴ The parameters resulting from our numerical procedure are listed in Table II for C, Si, and Ge, and in Table III for AlP, GaP, InP, AlAs, GaAs, InAs, AlSb, GaSb, and InSb. The corresponding energy eigenvalues and effective masses are summarized in Tables IV–VII and compared with experimental and quasiparticle results. Band structures are shown in Fig. 2 for diamond and silicon, and in Fig. 3 for germanium and gallium arsenide as a prototype example of a polar material. One of the main deficiencies of smaller nearest-neighbor TB models is that the transverse masses at X and L become too large or even infinite when only interactions among nearest neighbors are included. We consider the improved band shape on the surface of the Brillouin zone as a crucial test for the quality of our TB model, and this is the reason why we have included in the figures the part of the wave-vector pathway connecting several of these surface points, $X \rightarrow W \rightarrow K \rightarrow L \rightarrow W \rightarrow X$.

Following the work of Chadi,²⁵ spin-orbit interactions were added to the present model, including only the contribution from the p valence states, while the much smaller splittings of excited d states were neglected.²⁶ As in smaller TB models, the spin-orbit splittings in the crystal are larger than the atomic reference values by a factor of about 1.5.²⁵

The data presented in Tables IV–VII demonstrate that our results are in good agreement with experimental and quasiparticle calculations. The main features of the valence bands and the lowest two conduction bands are well reproduced, especially at Γ and X . For GaSb, the inversion $E(X_{6c}) > E(X_{7c})$, known from pseudopotential calculations, is reproduced.¹⁰ At the L point, deviations around the optically relevant gaps occur for the energetic positions of the highest valence band and second conduction band at L . We believe this systematic deviation cannot be overcome in a nearest-neighbor TB model, because an important invariant of fourth order in the wave number with symmetry $3(k_x^4 + k_y^4 + k_z^4) - k^4$ cannot be produced correctly. Its quantitative construction within a TB model would require interactions among more distant atoms. The adjustment of this invariant was found to be important for good agreement of a $15 \times 15 \mathbf{k} \cdot \mathbf{p}$ model with pseudopotential bands.³² This $\mathbf{k} \cdot \mathbf{p}$ model is based on Γ states arising from the wave vectors $(0,0,0)$, $\langle 1,1,1 \rangle$, and $\langle 2,0,0 \rangle$, so that it should have properties similar to our empirical TB model covering the same points, with the exception of a missing s^{**} band arising from $\langle 2,0,0 \rangle$, but including instead some approximate bands corresponding to higher reciprocal-lattice vectors. The masses calculated in our TB model agree with measurements except for the heavy-hole effective masses whose values are actually controversial even in experiments.³³

In a perfect cubic crystal, the on-site integrals evolve from the free-atomic term values corrected by the crystal-field potential. The differences between our s and p energies agree well with atomic reference calculations, especially for the nonpolar semiconductors.³⁴ For III-V semiconductors, the s - p splitting is up to 7% higher than in the corresponding atoms, with the exception of Sb, which deviates by 12%.^{35,36} This demonstrates that the chemistry of the highest occupied orbitals of the atoms is well conserved, as in smaller TB models.^{4,25} Conversely, the on-site d energies in Tables II and III scale with the energy unit of the reciprocal lattice, not

TABLE III. Empirical TB parameters for III-V semiconductors. The energy zero is taken at the valence-band maximum. The lattice constant a and the energy unit $E_{\langle 1,0,0 \rangle}$ are given at room temperature (Ref. 27); all other parameters are intended to be low-temperature values, in units of eV, with the energy zero at the valence maximum.

	AlP	GaP	InP	AlAs	GaAs	InAs	AlSb	GaSb	InSb
a (Å)	5.4635	5.4509	5.8687	5.660	5.6532	6.0583	6.1355	6.0959	6.4794
$E_{\langle 1,0,0 \rangle}$	5.0391	5.0624	4.3673	4.6953	4.7065	4.0982	3.9957	4.0478	3.5828
E_s^a	-5.3355	-5.3379	-5.3321	-5.9819	-5.9819	-5.9801	-4.9565	-4.9586	-4.9527
E_s^c	0.9573	-0.4005	0.3339	0.9574	-0.4028	0.3333	0.9521	-0.4003	0.3389
E_p^a	3.3471	3.3453	3.3447	3.5826	3.5820	3.5813	4.0739	4.0735	4.0797
E_p^c	6.3392	6.3844	6.4965	6.3386	6.3853	6.4939	6.3386	6.3801	6.4919
E_d	14.1717	14.0431	12.7756	13.0570	13.1023	12.1954	11.4691	11.5944	11.2647
E_{s^*}	20.5963	20.3952	18.8738	19.5133	19.4220	17.8411	16.4173	16.6388	16.1664
$ss\sigma$	-1.7403	-1.7049	-1.4010	-1.7292	-1.6187	-1.4789	-1.6179	-1.3671	-1.1290
$s^*s^*\sigma$	-3.6444	-3.5704	-3.6898	-3.6094	-3.6761	-3.8514	-3.3145	-3.2355	-3.2248
$s_a^*s_c\sigma$	-1.6448	-1.6034	-1.8450	-1.6167	-1.9927	-2.1320	-1.6983	-1.9813	-2.0042
$s_a^*s_c^*\sigma$	-1.4307	-1.6358	-1.2867	-1.2688	-1.5648	-1.2219	-1.2097	-1.6622	-1.8819
$s_a p_c \sigma$	2.6146	2.8074	2.1660	2.5175	2.4912	2.3159	2.5918	2.5624	2.5362
$s_c p_a \sigma$	2.7804	2.9800	2.6440	2.7435	2.9382	2.8006	2.9334	2.7093	2.6980
$s_a^* p_c \sigma$	2.0632	2.3886	2.5652	2.1190	2.1835	2.6467	2.4649	3.0164	2.7380
$s_c^* p_a \sigma$	2.3361	2.1482	2.0521	2.1989	2.2086	1.9012	1.8889	2.4596	2.3471
$s_a d_c \sigma$	-2.5253	-2.7840	-2.5559	-2.5535	-2.7333	-2.5828	-2.7920	-2.6143	-2.5635
$s_c d_a \sigma$	-2.1687	-2.3143	-2.2192	-2.3869	-2.4095	-2.4499	-2.0008	-2.4274	-2.3085
$s_a^* d_c \sigma$	-0.7810	-0.6426	-0.7912	-0.8064	-0.6906	-0.8497	-0.7307	-0.8557	-0.7371
$s_c^* d_a \sigma$	-0.7211	-0.6589	-0.8166	-0.7442	-0.6486	-0.8371	-0.7878	-0.8007	-0.8144
$pp\sigma$	4.0355	4.1988	4.0203	4.2460	4.4094	4.1188	4.1042	4.4500	4.1830
$pp\pi$	-1.3077	-1.4340	-1.2807	-1.3398	-1.4572	-1.3687	-1.5273	-1.6809	-1.4688
$p_a d_c \sigma$	-1.6750	-1.7911	-1.9239	-1.7240	-1.7811	-2.1222	-1.9819	-2.0377	-2.1487
$p_c d_a \sigma$	-1.8239	-1.8106	-1.8851	-1.7601	-1.8002	-2.0584	-1.9726	-2.2429	-2.1652
$p_a d_c \pi$	1.8760	1.8574	1.5679	1.7776	1.7821	1.5462	2.1292	1.9790	1.8462
$p_c d_a \pi$	2.1848	2.1308	1.7763	2.0928	2.0709	1.7106	1.8364	1.8670	1.8491
$dd\sigma$	-1.3479	-1.2268	-1.2482	-1.2175	-1.1409	-1.2009	-1.1395	-1.2492	-1.3052
$dd\pi$	2.3750	2.2752	2.1487	2.1693	2.2030	2.1820	2.1206	2.1970	2.0784
$dd\delta$	-1.8464	-2.0124	-1.6857	-1.7540	-1.9770	-1.7788	-1.7260	-1.7451	-1.4118
$\Delta_a/3$	0.0196	0.0301	0.0228	0.1721	0.1824	0.1763	0.3912	0.4552	0.4495
$\Delta_c/3$	0.0073	0.0408	0.1124	0.0072	0.0408	0.1248	0.0079	0.0432	0.1230

with the energy separation $E_d - E_p$ of the free atoms.²⁶ The very high on-site d energies can be understood by starting with realistic extended atomic d -wave functions. These wave functions would yield interaction matrix elements with more distant sites, and correspondingly nonvanishing overlap matrix elements. Diagonalizing everything except the nearest-neighbor interactions, the new on-site d energies of the orthogonal Wannier functions are renormalized and pushed up in energy by the elimination of interactions with the atomic orbitals at more distant positions and all overlap matrix elements.

The on-site d energies are about three energy units $E_{\langle 1,0,0 \rangle}$ above the average s energy, as expected from Sec. III. The chemical trend among AlP with $E_d - E_s = 3.25E_{\langle 1,0,0 \rangle}$ and

InSb with $E_d - E_s = 3.79E_{\langle 1,0,0 \rangle}$ is monotonous, and can be understood from the presence of occupied d orbitals in the core of the heavier atoms, pushing the empty free-electron-like d states to higher energies. For the s^* orbitals, the renormalization of the expected free-electron value $E_{s^*} - E_s = 4E_{\langle 1,0,0 \rangle}$ is more pronounced: among $E_{s^*} - E_s = 4.52E_{\langle 1,0,0 \rangle}$ for AlP and $E_{s^*} - E_s = 5.16E_{\langle 1,0,0 \rangle}$ for InSb. The increased influence of the core can be understood from the smaller value $E_{s^*} - E_s$ compared to the energetic separation of empty and occupied d states, if the latter are present at all. The nonpolar semiconductors Si and Ge show renormalizations similar to AlP and GaAs, respectively. Diamond is the only material with the opposite trend compared to the free-electron reference: $E_d - E_s = 2.45E_{\langle 1,0,0 \rangle}$ and $E_{s^*} - E_s$

TABLE IV. Comparison of energetic positions and masses obtained in the present work (TB) with experimental values (expt) and pseudopotential calculations in the GW approximation (PP) (Ref. 11), for Si, Ge, and C. All energies are in eV, and the reference energy is taken at the maximum of the valence band. The experimental data are from Ref. 27 unless indicated otherwise. Bands are assigned with representations in the double-group notation, except for the conduction bands at L , where the simple-group notation is also given for clarity.

	C		Si		Ge				
	TB	expt	PP	TB	expt	PP	TB	expt	PP
Γ_{6v}^+	-20.50	-21.	-21.35	-12.24	-12.5	-12.04	-12.68	-12.6	-12.84
$-\Delta_0$	0.00	0.00	0.0	-0.044	-0.044	0.0	-0.29	-0.30	0.0
Γ_{6c}^-	13.9	15.3	14.54	4.15	4.15	3.83	0.90	0.9	0.65
Γ_{7c}^-	7.35	7.3	7.63	3.36	3.35	3.39	3.04	3.01	3.21
Γ_{8c}^-	7.35	7.3	7.63	3.41	3.35	3.39	3.37	3.21	3.21
X_{5v}	-6.49		-6.69	-3.15	-2.90 ^a	-2.98	-3.37	-3.15	-3.16
X_{5c}	6.05	$X_{5v}^- + 12.5$	6.3	1.35	1.13	1.47	1.12	1.3	1.74
L_{6v}^-	-2.76		-2.98	-1.12	-1.2	-1.24	-1.37	-1.4	-1.47
$L_{4,5v}^-$	-2.76		-2.98	-1.08	-1.2	-1.24	-1.12	-1.4	-1.47
$L_{6c}^+(L_{1c}^+)$	9.73	$L_{4,5v}^- + 12.5$	10.63	2.14	2.40 ^a	2.26	0.74	0.74	0.98
$L_{6c}^+(L_{3c}^+)$	9.30	$L_{4,5v}^- + 12.0$	10.23	4.39	4.15 ^a	4.33	3.99	4.3	4.57
$m(\Gamma_{6c}^-)$							0.038	0.038	
$m_r(\Delta_{\min})$	0.33	0.36		0.22	0.1905		0.280		
$m_r(L_{6c}^+)$				0.16			0.083	0.081	
Δ_{\min}	5.50	5.48	5.67	1.17	1.17	1.31	1.00		

^aReference 28.

$=3.33E_{(1,0,0)}$, both below the expected values. Nevertheless, the general laws derived for the free electrons dominate the expected ordering of the atomic levels even for diamond: $E_s^* = E_{3s} > E_d = E_{3d}$.

B. Total and local density of states

We calculated the electronic density of states (DOS) and the local density of states (LDOS) projected on the atomic basis functions. Our results for GaAs are presented in Fig. 4. The energetically lowest peak from -13 to -10 eV arises

TABLE V. Comparison of energetic positions and masses obtained in the present work (TB) with experimental values (expt) (Ref. 27) and pseudopotential calculations in the GW approximation (PP) (Ref. 30), for AlP, GaP, and InP. All energies are in eV, and the reference energy is taken at the maximum of the valence band. Bands are assigned with representations in the double-group notation, and the origin is chosen on the anion site.

	AlP		GaP		InP	
	TB	expt	PP	TB	expt	PP
Γ_{6v}	-11.823		-12.07	-12.365	-12.3	-12.83
$-\Delta_0$	-0.040		0.0	-0.080	-0.080	0.0
Γ_{6c}	3.630	3.63	4.38	2.895	2.895	2.85
Γ_{7c}	4.525		5.72	4.460	4.87	5.03
Γ_{8c}	4.553		5.72	4.553	4.87	5.03
X_{6v}	-2.484		-2.31	-2.849	-2.7, -3.0	-2.78
X_{7v}	-2.466		-2.31	-2.845	-2.7, -3.0	-2.78
X_{6c}	2.504	2.505	2.59	2.349	2.350	2.55
X_{7c}	2.936		3.56	2.701	2.75	2.81
L_{6v}	-0.986		-0.85	-1.133	-1.2, -0.9	-1.16
$L_{4,5v}$	-0.957		-0.85	-1.069	-1.2, -0.9	-1.16
L_{6c}	3.121		3.90	2.556	2.563	2.67
L_{6c}	5.166		6.05	5.244	5.50	5.87
$m(\Gamma_{6c})$	0.187			0.128		0.074
$m_r(X_{6c})$	0.247		0.212 ^a	0.255	0.254	0.285
$m_r(L_{6c})$	0.189			0.150		0.135

^aReference 27, calculated.

TABLE VI. Like Table V, but for AlAs, GaAs, and InAs.

	AlAs		GaAs		InAs				
	TB	expt	PP	TB	expt	PP	TB	expt	PP
Γ_{6v}	-12.020		-12.41	-12.910	-13.1	-13.03	-12.188	-12.3	-12.10
$-\Delta_0$	-0.300	-0.30	-0.27	-0.340	-0.341	-0.34	-0.380	-0.38	-0.38
Γ_{6c}	3.130	3.13	2.88	1.519	1.519	1.22	0.418	0.418	0.31
Γ_{7c}	4.569	4.54	5.14	4.500	4.53	4.48	4.252	4.39	4.51
Γ_{8c}	4.725	4.69	5.14	4.716	4.716	4.48	4.580	4.39	4.51
X_{6v}	-2.760	-2.41	-2.44	-3.109	-2.88	-2.91	-2.654	-2.4	-2.49
X_{7v}	-2.565	-2.41	-2.44	-2.929	-2.80	-2.91	-2.546	-2.4	-2.49
X_{6c}	2.223	2.229	2.14	1.989	1.98	1.90	2.176		2.01
X_{7c}	2.584	2.579	3.03	2.328	2.35	2.47	2.441		2.50
L_{6v}	-1.191		-0.99	-1.330	-1.42	-1.28	-1.124	-0.9	-1.13
$L_{4,5v}$	-0.983		-0.99	-1.084	-1.20	-1.28	-0.830	-0.9	-1.13
L_{6c}	2.581	2.54	2.91	1.837	1.85	1.64	1.691		1.43
L_{6c}	5.069		5.59	5.047	5.47	5.40	4.723		5.32
$m(\Gamma_{6c})$	0.156			0.067	0.067		0.024	0.023	
$m_t(X_{6c})$	0.237	0.19		0.237	0.27		0.278		
$m_t(L_{6c})$	0.155			0.117	0.075		0.110		

from the As 4s state with a small contribution from the cation *s*, *p*, and *d* states. The threshold at -7 eV is the absolute minimum of the second valence band, and the corresponding wave functions have *sp*-bonding character, arising from the mixing of Ga 4s and As 4p states. At -4.1 eV the absolute minimum of the third valence band on the surface of the Brillouin zone occurs, and the peak near -3 eV corresponds to the position of the two highest valence bands at *X*, in agreement with experiment. These bands are mainly composed of *p* and *d* states, and at the valence maximum, the *s* contribution vanishes for symmetry reasons. The lowest conduction band at Γ consists mainly of antibonding combinations of *s* orbitals with a marked anion character ($s_a + s_a^*$

=54%). This is in contrast with the older *sp* TB result giving a larger cation contribution ($s_c = 70\%$),³ but agrees well with pseudopotential calculations.^{9,12} Using a smaller *spd* basis, the improvement of the conduction-band wave function is lost, and the old *sp* result is reproduced. The change of $E_p - E_s$ by about 2 eV (0.5 $E_{(1,0,0)}$) needed in the *spd* basis destroys the correspondence with atomic *s* orbitals and the transferability.

At higher energies, the DOS of the conduction band displays a free-electron-like character all around the surface of the Brillouin zone, reflected by the strong admixture of all atomic symmetries *s*, *p*, and *d*. Compared to self-consistent pseudopotential calculations, the calculated DOS and LDOS

TABLE VII. Like Table V, but for AlSb, GaSb, and InSb.

	AlSb		GaSb		InSb				
	TB	expt	PP	TB	expt	PP	TB	expt	PP
Γ_{6v}	-11.242		-11.10	-11.838	-11.74	-11.72	-11.435	-11.73	-10.91
$-\Delta_0$	-0.673	-0.673	-0.673	-0.756	-0.756	-0.76	-0.803	-0.803	-0.80
Γ_{8v}	0.0	0.0	0.0	0.0	0.0	0.0	0.0	0.0	0.0
Γ_{6c}	2.384	2.384	2.23	0.811	0.8113	0.62	0.235	0.235	0.08
Γ_{7c}	3.663	3.740	3.52	3.437	3.20	3.11	3.503	3.37	3.16
Γ_{8c}	3.913	4.00	3.82	3.839	3.54	3.32	4.000	3.74	3.55
X_{6v}	-2.691	-2.80 ^a	-2.54	-3.401	-3.10	-2.73	-2.722	-2.4	-2.56
X_{7v}	-2.263	-2.40 ^a	-2.54	-2.931	-2.86	-2.97	-2.317	-2.4	-2.24
X_{6c}	1.692	1.69	1.64	1.392	1.40	1.50	1.756	1.79	1.50
X_{7c}	1.901		1.84	1.226	1.24	1.15	1.864		1.57
L_{6v}	-1.13		-1.48	-1.480	-1.53	-1.56	-1.30	-1.4	-1.46
$L_{4,5v}$	-0.67		-1.06	-0.930	-1.10	-1.14	-0.701	-0.9	-0.96
L_{6c}	2.44	2.33	1.84	0.897	0.897	0.79	1.227		0.76
L_{6c}	3.983		4.29	4.005	4.36	4.11	4.059		4.09
$m(\Gamma_{6c})$	0.109			0.041	0.041		0.012	0.0136	
$m_t(X_{6c})$	0.223	0.23		0.207	0.22		0.218		
$m_t(L_{6c})$	0.120			0.081	0.11		0.082	0.09	

^aReference 31.

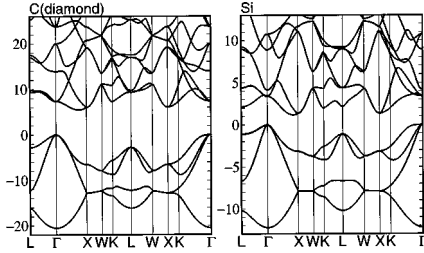


FIG. 2. Band structure for C (diamond) and Si. The model parameters are given in Table II, and some values of band energies and masses in Table IV.

show good agreement and underline the quality of the wavefunction symmetries obtained in the present model.³⁶ The total bond character summed over all valence bands is approximately $s^{1.41}p^{2.37}d^{0.22}$, which is nearly invariant for all materials investigated. As chemical trends are weak, this can be considered as an intrinsic property of the tetrahedral bond configuration, so that the sp^3 symmetry always mentioned is only approximately correct. sp^3 bonding does not occur in any energetic region when averaging over each energy shell.

C. Dependence of band energies on TB parameters

In order to investigate the dependence of the band energies on the model parameters, we compute the partial derivatives of some energies with respect to the on-site energies, e.g., $\partial E(\Gamma_{6c})/\partial E_s^a$, and with respect to two-center integrals, e.g., $\partial E(\Gamma_{6c})/\partial(ss\sigma)$. The first give the composition of the wave function directly, and, because two representations for d states occur, we calculate also the corresponding decomposition. Results for GaAs are found in Table VIII, and the decompositions of the wave functions are in good agreement with pseudopotential calculations.¹²

From the Hellmann-Feynman theorem, the following relation between the Hamiltonian matrix elements H_{ij} and the resulting eigenvalues $E_n(\mathbf{k})$ can be deduced,³⁷

$$E_n(\mathbf{k}) = \sum_{i,j} H_{ij} \frac{\partial E_n(\mathbf{k})}{\partial H_{ij}}, \quad (36)$$

where n, \mathbf{k} and i, j label, respectively, the band states and the symmetry of the Bloch functions. Within the Slater-Koster approach, H_{ij} depends linearly on the on-site energies E_l and two-center integrals $ij\kappa$ (all labeled E_l for brevity),

$$H_{ij} = \sum_l E_l \frac{\partial H_{ij}}{\partial E_l}. \quad (37)$$

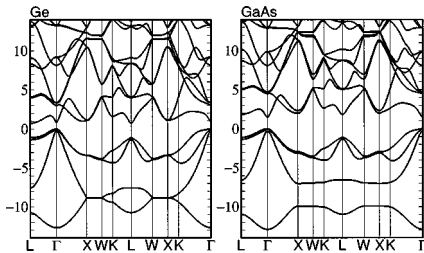


FIG. 3. Band structure for Ge and GaAs. The model parameters are given in Tables II and III, and some values of band energies and masses in Tables IV and VI.

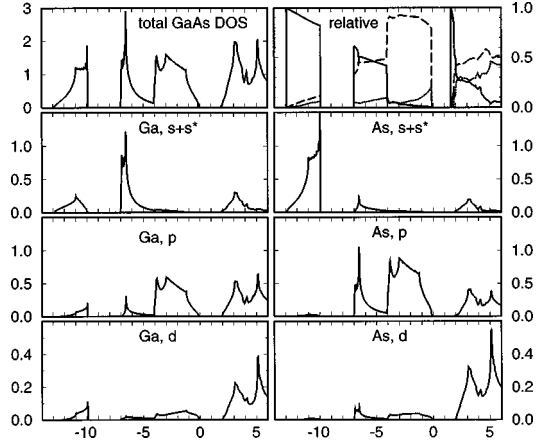


FIG. 4. Total and partial density of states (DOS) for GaAs. Upper left panel: Total density of states, upper right panel: relative DOS of the corresponding symmetries (s : solid line; p : dashed; d : dotted). Other panels: DOS divided into contributions of s , p , and d symmetries, and cation (left) and anion (right), as labeled. The DOS is calculated without spin-orbit splitting.

Using this expression and Eq. (36), we can relate each eigenvalue $E_n(\mathbf{k})$ linearly to the model parameters:

$$E_n(\mathbf{k}) = \sum_l E_l \frac{\partial E_n(\mathbf{k})}{\partial E_l}. \quad (38)$$

While this relation is strictly valid for each semiconductor, we can use it for interpolating between different types of III-V materials. Assuming that the partial derivatives in Eq. (38) show only a weak material dependence, we calculate them for the reference material GaAs (compare Table VIII), and use the TB parameters E_l for the other types of semiconductors. This procedure works surprisingly well, and it is useful to relate chemical trends in band positions to the corresponding trends in the TB parameters.

The conduction minimum Γ_{6c} shows a monotonous decrease with increasing cation or anion size. The main part of the chemical trend is already recovered with the three largest derivatives,

$$\frac{\partial E(\Gamma_{6c})}{\partial (ss\sigma)} ss\sigma + \frac{\partial E(\Gamma_{6c})}{\partial (s_a^* s_c \sigma)} s_a^* s_c \sigma + \frac{\partial E(\Gamma_{6c})}{\partial (s_a s_c^* \sigma)} s_a s_c^* \sigma, \quad (39)$$

while the derivatives with respect to the on-site energies make a much smaller contribution to the material dependence of Γ_{6c} . The general feature that interaction matrix elements have a stronger influence than the on-site energies is also observed for other band positions, underlining that the dependence of energy bands on volume effects can be described by considering only the variation of the two-center integrals in the strain Hamiltonian, neglecting the on-site energy changes. The dependence of the X_{6c} conduction minimum on the TB parameters is already rather complicated. As the 10×10 coupling matrices for the Δ_1 bands decompose into two 5×5 subblocks for X_{6c} and X_{7c} , only s_a , s_a^* , p_c , $d_a(\Gamma_3)$, and $d_c(\Gamma_4)$ contribute to the X_{6c} -state. The main part of the dependence of the X_{6c} conduction minimum comes from the interaction parameters among $\{s, s^*\}$ and

TABLE VIII. Partial derivatives of valence and conduction energies with respect to on-site energies and interaction parameters, for GaAs. Entries vanishing due to symmetry restrictions are denoted with $-$.

E (eV)	Γ_{6v}	Γ_{6c}	X_{6c}	L_{6c}	Γ_{8v}	Γ_{8c}	X_{6v}	$L_{4,5v}$
	-12.910	1.519	1.989	1.837	0.0	4.716	-2.929	-1.084
E_s^a	0.564	0.411	0.029	0.145	-	-	-	-
E_s^c	0.303	0.456	-	0.297	-	-	-	-
$E_{s^*}^a$	0.065	0.128	0.025	0.043	-	-	-	-
$E_{s^*}^c$	0.068	0.005	-	0.003	-	-	-	-
E_p^a	-	-	-	0.147	0.553	0.290	0.580	0.589
E_p^c	-	-	0.458	0.239	0.234	0.510	0.416	0.350
E_d^a	-	-	0.325	0.090	0.084	0.169	0.001	0.022
E_d^c	-	-	0.163	0.037	0.129	0.032	0.002	0.038
$d_a(\Gamma_3)$	-	-	0.325	-	-	-	-	0.007
$d_c(\Gamma_3)$	-	-	-	-	-	-	-	0.013
$d_a(\Gamma_4)$	-	-	-	0.090	0.084	0.169	0.001	0.015
$d_c(\Gamma_4)$	-	-	0.163	0.037	0.129	0.032	0.002	0.025
$ss\sigma$	3.308	-3.463	-	-0.830	-	-	-	-
$s^*s^*\sigma$	0.532	0.200	-	-0.046	-	-	-	-
$s_a^*s_c\sigma$	1.122	1.934	-	0.450	-	-	-	-
$s_a s_c^*\sigma$	1.568	-0.359	-	0.085	-	-	-	-
$s_a p_c \sigma$	-	-	0.529	0.743	-	-	-	-
$s_c p_a \sigma$	-	-	-	0.836	-	-	-	-
$s_a^* p_c \sigma$	-	-	-0.497	-0.403	-	-	-	-
$s_c^* p_a \sigma$	-	-	-	-0.085	-	-	-	-
$s_a d_c \sigma$	-	-	0.315	0.291	-	-	-	-
$s_c d_a \sigma$	-	-	-	0.653	-	-	-	-
$s_a^* d_c \sigma$	-	-	-0.296	-0.158	-	-	-	-
$s_c^* d_a \sigma$	-	-	-	-0.067	-	-	-	-
$pp\sigma$	-	-	-	-0.250	-0.959	1.003	-1.310	-1.212
$pp\pi$	-	-	-	0.998	-1.917	2.007	1.310	-0.606
$p_a d_c \sigma$	-	-	-	-0.098	0.712	0.214	0.100	0.325
$p_c d_a \sigma$	-	-	-	-0.194	0.374	0.818	0.060	0.195
$p_a d_c \pi$	-	-	-	-0.226	-0.822	-0.247	0.058	-0.379
$p_c d_a \pi$	-	-	-2.058	-0.451	-0.432	-0.945	0.034	-0.219
$dd\sigma$	-	-	-	0.076	0.278	-0.174	0.005	0.052
$dd\pi$	-	-	-0.708	-0.102	0.185	-0.116	-0.002	0.086
$dd\delta$	-	-	0.708	-0.204	0.371	-0.233	-0.003	-0.021

$\{p,d\}$ and from E_d . We note that both $d_a(\Gamma_3)$ and $d_c(\Gamma_4)$ basis states contribute significantly to the X_{6c} wave function, underlining the necessity to include both types of d states in the TB basis when modeling surface points of the Brillouin zone. For the L_{6c} conduction minimum, the dependence on the material parameters is so complicated that no evident chemical trends can be extracted. Even in this very complicated case, where all partial derivatives contribute, the agreement of Eq. (38) using the derivatives for GaAs and the TB parameters of the other materials, with the corresponding L_{6c} energies, is remarkable. L_{6c} is never the absolute conduction minimum in the III-V materials investigated: Only the order-

ings $X_{6c} < L_{6c} < \Gamma_{6c}$ (AlP, AlAs, AlSb, GaP) and $\Gamma_{6c} < L_{6c} < X_{6c}$ (GaAs, GaSb, InP, InAs, InSb) occur.

The valence bands show nearly 100% p character at L and X , while at Γ , the d admixture of 21% is in good agreement with pseudopotential calculations.¹² These compositions of the valence wave functions are typical of all semiconductors investigated, so that the d contribution of about $\frac{1}{5}$ to the valence maximum can be regarded as an intrinsic property of the diamond and zinc-blende semiconductors. The small- d contributions at X and L are the reason why the positions of the highest valence bands X_{6v} and $L_{4,5v}$ depend mainly on the p - p interactions and the on-site p energies. As

the material dependencies of these quantities are not very pronounced, the corresponding band energies show much smaller chemical trends than the conduction minima, especially Γ_{6c} .

V. DEFORMATION POTENTIALS

To achieve a complete description of the interaction parameters, we scale the Hamiltonian matrix elements by calculating the dependence of energy bands on volume effects. In a TB Hamiltonian, strain effects can be included by scaling the matrix elements with respect to the bond-angle distortions and bond-length changes, allowing for the calculation of strain effects for any wave vector with the same accuracy. Bond-angle distortions are determined by elasticity theory and incorporated into the Hamiltonian matrix elements via the phase factors in the Slater-Koster definitions. The influence of changes of the on-site Hamiltonian matrix elements on the resulting band structure is difficult to evaluate because two different terms contribute: the energy level of the free atom and the crystal field. As mentioned above, the variation of the band energies with the one-center integrals E_l is weak, so that the main dependence on volume effects should be recovered, keeping the on-site energies constant. The dependence of the two-center integrals $ij\kappa$ on bond length is considered using a generalization of Harrison's d^{-2} law,³⁹

$$ij\kappa(d) = ij\kappa(d_0) \left(\frac{d_0}{d} \right)^{n_{ijk}}, \quad (40)$$

where d (d_0) is the strained (unstrained) interatomic distance. n_{ijk} are orbital-dependent exponents reflecting the localization of the atomic wave functions i and j near the nuclei. In a minimal sp basis, Harrison chose all coefficients n_{ijk} equal to 2, consistent with the free-electron spectra. The strain Hamiltonian obtained this way provides a fairly good description of the positive pressure coefficient $dE(\Gamma_{6c} - \Gamma_{8v})/dp$ of the direct gap, but it predicts an erroneous positive pressure coefficient of the indirect gap $dE(X_{6c} - \Gamma_{8v})/dp$, which should be negative. This failure is easily understood when considering the sp expressions of the Γ and X energies for the diamond structure, neglecting the dependence of the spin-orbit splitting on strain:³

$$E(\Gamma_{8c}^+, \Gamma_{8v}^-) = E_p \pm V_{xx}, \quad (41)$$

$$E(X_{6c}, X_{8v}) = \frac{E_s + E_p}{2} \pm \sqrt{\left(\frac{E_p - E_s}{2} \right)^2 + V_{sp}^2}. \quad (42)$$

The dependence on pressure is then determined by the increase of the interaction parameters with decreasing interatomic distance: The lower bonding state of each pair will be pushed down in energy, while the higher antibonding state will be pushed up. We obtain the following volume deformation potentials:

$$a(\Gamma_{8v}^-) = \frac{1}{3} \frac{\partial E(\Gamma_{8v}^+)}{\partial \ln(d)} = \frac{2}{3} V_{xx} > 0, \quad (43)$$

$$a(\Gamma_{8c}^+) = -a(\Gamma_{8v}^-), \quad (44)$$

$$a(X_{6c}) = \frac{1}{3} \frac{\partial E(X_{6c})}{\partial \ln(d)} = -\frac{4}{3} \frac{V_{sp}^2}{E(X_{6c}) - E(X_{8v})} < 0. \quad (45)$$

Normalizing these deformation potentials with the bulk modulus B_0 yields a positive pressure coefficient for the indirect gap,

$$\frac{\partial}{\partial p} [E(X_{6c}) - E(\Gamma_{8v}^-)] = -\frac{a(X_{6c}) - a(\Gamma_{8v}^-)}{B_0} > 0, \quad (46)$$

in sharp contrast with the sign observed.²⁷ Partly, these deficiencies can be overcome in an sps^* model including more sophisticated distance laws than $n_{ijk} = 2$.³⁹ However, owing to the large d component of the conduction-band wave function at X , any agreement would be fortuitous. Including the d states, the required change of sign of $a(X_{6c})$ and the corresponding pressure coefficient is simply related to the fact that the corresponding wave function contains a large contribution of d states (compare Table VIII), which has entirely bonding character as shown in Fig. 1: The surroundings of the X point have the lowest bonding d states. The d -symmetric part of the X_{6c} wave function will therefore be pushed down in energy under pressure, yielding a negative pressure coefficient of X_{6c} , and a negative pressure coefficient of the indirect gap.

In order to overcome the inherent limitations of smaller TB models, we shall derive the distance laws of our empirical TB parameters in the $spds^*$ basis from various deformation potentials of several band positions at Γ , X , and L . In a nearest-neighbor approximation, shear deformation potentials are not n_{ijk} dependent. Uniaxial [001] strain induces a tetragonal crystal field which lifts the degeneracy of the xy (z) and xz , yz (x , y) atomic levels. For convenience, we consider only the d states, and assuming a linear dependence of the on-site energies on the strain tensor ϵ , we obtain

$$E_{xy} = E_d [1 + 2b_d(\epsilon_{zz} - \epsilon_{xx})], \quad (47)$$

$$E_{xz} = E_{yz} = E_d [1 - b_d(\epsilon_{zz} - \epsilon_{xx})],$$

where b_d is the shear parameter of the d states fitted to reproduce the uniaxial deformation b of the valence-band edge. The average $d(\Gamma_4)$ energy in Eq. (47) remains unchanged, i.e., we do not consider volume effects. The numerical values derived are given in Table IX together with the exponents of the interaction parameters. Anion-cation and cation-anion interactions of the same type are assumed to fulfill the same distance law, e.g., $n_{s_a p_c \sigma} = n_{s_c p_a \sigma} = n_{sp\sigma}$. In the numerical fitting procedure, we achieve good agreement with pseudopotential calculations and experimental deformation potentials (see Table X). Pressure coefficients of valence and conduction states were fitted separately, when available, but only the pressure dependence of the gaps is shown. The pressure coefficient $\partial E(\Gamma_{8v}^- - \Gamma_{8c}^+)/\partial p$ for Si is in close agreement with pseudopotential results,²⁹ while, on an sp or sps^* basis, $a(\Gamma_{8c}^+)$ has the opposite sign of $a(\Gamma_{8v}^-)$; compare Eqs. (43) and (44). Another point to be emphasized is that the TB calculation gives for all III-V semiconductors

TABLE IX. Empirical distance laws $n_{ijk\kappa}$ of the TB parameters for Si, Ge, and III-V semiconductors, fitted to various deformation potentials as explained in the text. The exponents $n_{ss^*\sigma}$ and $n_{s^*s^*\sigma}$ were set to zero, and $n_{dd\sigma}$, $n_{dd\pi}$, $n_{dd\delta}$, and $n_{s^*d\sigma}$ were fixed to the free-electron value of 2.

$ijk\kappa$	Si	Ge	AlP	GaP	InP	AlAs	GaAs	InAs	AlSb	GaSb	InSb
$ss\sigma$	3.672	3.631	3.041	3.379	3.113	3.120	3.640	3.348	3.245	4.041	3.991
$sp\sigma$	2.488	3.713	3.408	3.360	3.582	3.564	3.582	3.662	3.702	3.644	3.671
$pp\sigma$	2.187	2.030	2.138	2.124	1.825	2.051	2.045	1.498	1.763	1.524	1.348
$pp\pi$	3.711	4.025	3.871	3.927	4.153	3.869	4.126	4.259	4.152	4.203	4.297
$sd\sigma$	1.869	1.931	1.956	1.971	1.993	1.871	1.954	1.776	1.721	1.799	1.778
$s^*p\sigma$	1.919	1.830	1.816	1.819	1.692	1.799	1.712	1.762	1.772	1.770	1.755
$pd\sigma$	1.830	1.759	1.843	1.832	1.772	1.858	1.827	1.740	1.797	1.753	1.734
$pd\pi$	2.093	1.872	1.864	1.837	1.732	1.874	1.651	1.696	1.557	1.642	1.675
b_d	0.443	0.243	0.660	0.649	0.572	0.536	0.655	0.488	0.420	0.370	0.302

deformation potentials $a(X_{6c}) > a(X_{7c})$ for the lowest two conduction states at X , in agreement with pseudopotential results.³⁵

The distance laws can be divided into four groups. For the first, the exponents were set to zero because we do not expect a large influence of the corresponding parameters on our results, or because reliable information on high bands is missing. The corresponding exponents are $n_{ss^*\sigma} = n_{s^*s^*\sigma} = 0$. The second group concerns the high bands, and their exponents were fixed to Harrison's free-electron distance law: $n_{dd\sigma} = n_{dd\pi} = n_{dd\delta} = n_{s^*d\sigma} = 2$. These interactions guarantee that the high-energy parts of the band structure scale with $E_{\langle 1,0,0 \rangle}$, as the free electrons. For the third group, the exponents are still of the order of 2, but show pronounced chemical trends; compare Table IX. They apply to TB parameters describing the interaction among one of the low-lying states s or p and one of the high-lying states d or s^* . The fourth group contains the interactions within the subset $\{s,p\}$. They are known to be responsible for the main chemical trends for the valence bands, as they contribute about 94% to the bond-

ing orbitals (see Sec. IV B). The corresponding exponents turn out to be very high, of the order 3–4.5, values which are in rough agreement with exponents derived in cluster calculations.⁴⁰ Because the electron densities of the s and p states are localized much more closely to the nuclei than the free-electron-like d and s^* states, the corresponding two-center interaction matrix elements within the subset $\{s,p\}$ should in fact have the steepest distance dependence, as observed in our results.

VI. CONCLUSION AND OUTLOOK

With an empirical $sp^3d^5s^*$ nearest-neighbor TB model, we obtained a quantitatively correct description of the valence bands and the lowest two conduction bands, both in terms of energetic positions and band curvatures. The d states were found to be of crucial importance for the lowest two conduction bands at X , and the composition of the corresponding wave functions was in good agreement with pseudopotential results. The distance dependences of the in-

TABLE X. Pressure coefficients of band gaps for Si, GaAs, and GaSb, given in meV/Kbar, and deformation potentials b and $E_2(X)$ in eV. E_2 is calculated at the absolute minimum of the conduction band along Δ for Si, and at X for GaAs and GaSb.

	Si			GaAs			GaSb			
	TB	expt	PP	TB	expt	PP	TB	expt	PP	
$dE_0(\Gamma)/dp$	12.0			12.2 ^a	11.4	11.3	10.3 ^b	13.5	14.8	14.3 ^b
$dE'_0(\Gamma)/dp$	0.53			0.53 ^a						
$dE_1(L)/dp$	5.4	5.2		6.8	7.2		7.2	7.35		
$dE_2(X)/dp$	2.0	2.9		4.0	5.6		6.44	6.08		
$dE_g^{\text{ind}}(\Gamma_{8v} - X_{6c})/dp$	-1.8	-1.6	-1.68 ^a	-2.4	-1.8	-2.2 ^b	-3.6		-3.4 ^b	
$dE_g^{\text{ind}}(\Gamma_{8v} - X_{7c})/dp$	“	“	“	-0.1		-0.3 ^b	-2.0		-1.8 ^b	
$dE_g^{\text{ind}}(\Gamma_{8v} - L_{6c})/dp$	4.32		4.06 ^a	4.6	5.5	3.9 ^b	4.8	5.0	4.3 ^b	
b	-2.11	-2.10	-2.35 ^c	-1.69	-1.7	-1.90 ^c	-1.95	-2.0		
$E_2(\Delta)$ or $E_2(X)$	9.0	8.7	9.16 ^c	6.2	6.5 ^d	8.6 ^c , 6.3 ^e	6.5			

^aReference 29.

^bReference 35.

^cReference 38.

^dReference 45.

^eReference 27, calculated.

teraction parameters were derived from various deformation potentials. A major improvement compared to smaller TB models was the correct sign and magnitude of the deformation potential of the conduction band at X , directly related to the large d component of the wave function. Because all deformation potentials investigated have reasonable magnitudes, a generalization of the present model to strained superlattices is straightforward and has already been applied to AlAs/GaAs superlattices.⁴¹

A further extension concerns the combination of the present achievements with *ab initio* TB methods, where atomiclike wave functions are used.^{42,43} The necessity to choose unusual on-site energies in the present work, and the δ -like potentials used in muffin-tin methods,⁴⁴ demonstrate that the on-site energies of models based on atomiclike wave functions do not necessarily coincide with the atomic energy levels. This can be possibly exploited to achieve further improvements for the conduction bands. This would yield the possibility to use realistic sets of parameters where the wave functions are *ab initio* and on-site parameters are empirical. A better modeling of crystallization processes, surface reconstruction, and optical properties of clusters can be expected.

ACKNOWLEDGMENTS

The authors thank P. Vogl for unpublished pseudopotential calculations, J.-C. Vallet for help with MATHEMATICA, and P. Vogl and A. Papaconstantopoulos for clarifying discussions. This work was supported in part by the Commission of the European Union, and the Deutsche Forschungsgemeinschaft.

APPENDIX

The abbreviations used in the coupling Hamiltonian $H(\Delta_3)$ in Eq. (11) will be given below:

$$V_{dd}(\Delta_3) = \frac{4}{9}(3dd\sigma + 2dd\pi + 4dd\delta)\cos\frac{ka}{4} - i\frac{4}{9}(3dd\sigma - dd\pi - 2dd\delta)\sin\frac{ka}{4}, \quad (A1)$$

$$V_{pd}^{ac}(\Delta_3) = -\frac{4}{3}\left(P_a - \frac{2}{\sqrt{3}}P_ad_c\pi\right)\cos\frac{ka}{4} + i\frac{4}{3}\left(P_ad_c\sigma + \frac{1}{\sqrt{3}}P_ad_c\pi\right)\sin\frac{ka}{4}, \quad (A2)$$

$$V_{pd}^{ca}(\Delta_3) = \frac{4}{3}\left(P_cd_a\sigma - \frac{2}{\sqrt{3}}P_cd_a\pi\right)\cos\frac{ka}{4} + i\frac{4}{3}\left(P_cd_a\sigma + \frac{1}{\sqrt{3}}P_cd_a\pi\right)\sin\frac{ka}{4}, \quad (A3)$$

$$V_{pp}(\Delta_3) = V_{xx}\cos\frac{ka}{4} - iV_{xy}\sin\frac{ka}{4}, \quad (A4)$$

where

$$V_{xx} = \frac{4}{3}(pp\sigma + 2pp\pi), \\ V_{xy} = \frac{4}{3}(pp\sigma - pp\pi). \quad (A5)$$

*Present address: Institut für Physik, Technische Universität Chemnitz, D-09107 Chemnitz, Germany.

¹J. C. Slater and G. F. Koster, Phys. Rev. **94**, 1498 (1954).

²D. J. Chadi and M. L. Cohen, Phys. Status Solidi B **68**, 405 (1975).

³W. A. Harrison, *Electronic Structure and Properties of Solids* (Freeman, San Francisco, 1980).

⁴P. Vogl, H. P. Hjalmarson, and J. D. Dow, J. Phys. Chem. Solids **44**, 365 (1983).

⁵J. A. Majewski and P. Vogl, Phys. Rev. B **35**, 9666 (1987).

⁶A. Zunger and M. L. Cohen, Phys. Rev. B **20**, 4082 (1979).

⁷G. P. Kekker, Phys. Rev. B **24**, 3468 (1981).

⁸G. B. Bachelet and N. E. Christensen, Phys. Rev. B **31**, 879 (1985).

⁹S. L. Richardson, M. L. Cohen, S. G. Louie, and J. R. Chelikowsky, Phys. Rev. B **33**, 1177 (1986).

¹⁰S. L. Richardson and M. L. Cohen, Phys. Rev. B **35**, 1388 (1987).

¹¹M. Röhlffing, P. Krüger, and J. Pollmann, Phys. Rev. B **48**, 17791 (1993).

¹²P. Boguslawsky and I. Gorczyca, Semicond. Sci. Technol. **9**, 2169 (1994).

¹³Y. C. Chang and D. E. Aspnes, Phys. Rev. B **41**, 12002 (1990).

¹⁴M. Graf and P. Vogl, Phys. Rev. B **51**, 4940 (1995).

¹⁵B. Sporkmann and H. Bross, Phys. Rev. B **49**, 10869 (1994).

¹⁶J. Callaway, *Energy Band Theory* (Academic, New York, 1961).

¹⁷F. Bassani and G. Pastori-Parravicini, *Electronic States and Optical Transitions in Solids* (Pergamon, London, 1975).

¹⁸F. Herman, Phys. Rev. **93**, 1214 (1954).

¹⁹F. Bassani, in *Physics of III-V Compounds* edited by R. K. Willardson and A. C. Beer, Semiconductors and Semimetals Vol. 1 (Academic, New York, 1966), p. 33.

²⁰G. Dresselhaus, Phys. Rev. **100**, 580 (1955).

²¹P. Y. Yu and M. Cardona, *Fundamentals of Semiconductors* (Springer, Berlin, 1996).

²²S. Froyen and W. A. Harrison, Phys. Rev. B **20**, 2420 (1979).

²³W. A. Harrison and S. Froyen, Phys. Rev. B **21**, 3214 (1980).

²⁴D. A. Papaconstantopoulos, A. Pasturel, J. P. Julien, and F. Cyrot-Lackmann, Phys. Rev. B **40**, 8844 (1989).

²⁵D. J. Chadi, Phys. Rev. B **16**, 790 (1977).

²⁶D. M. Bylander and L. Kleinman, Phys. Rev. B **34**, 5280 (1986).

²⁷*Semiconductors: Group IV Elements and III-V Compounds*, edited by O. Madelung, Landolt-Börnstein, New Series, Group III, Vol. 17, Pt. a (Springer, Berlin, 1982); *Semiconductors: Intrinsic Properties of Group IV Elements and III-V, II-VI and I-VII Compounds*, edited by O. Madelung, Landolt-Börnstein, New Series, Group III, Vol. 22, Pt. a (Springer, Berlin, 1987).

²⁸D. Straub, L. Ley, and F. J. Himpsel, Phys. Rev. Lett. **54**, 142 (1985).

²⁹X. Zhu, S. Fahy, and S. G. Louis, Phys. Rev. B **39**, 7840 (1989).

³⁰X. Zhu and S. G. Louis, Phys. Rev. B **39**, 7840 (1991).

³¹D. H. Ehlers, F. U. Hillebrecht, C. T. Lin, E. Schönherr, and L. Ley, Phys. Rev. B **40**, 3812 (1989).

³²L.-W. Wang and A. Zunger, Phys. Rev. B **54**, 11417 (1996).

³³W. Nakawski, Physica B **210**, 1 (1995).

³⁴G. B. Bachelet and M. Schlüter, Phys. Rev. B **25**, 2103 (1982).

³⁵S.-H. Wei and A. Zunger, Phys. Rev. B **39**, 3279 (1989).

- ³⁶R. Magri, S. Froyen, and A. Zunger, Phys. Rev. B **44**, 7947 (1991).
- ³⁷S. B. Singh and C. A. Singh, Am. J. Phys. **57**, 894 (1989).
- ³⁸C. G. Van de Walle, Phys. Rev. B **39**, 1871 (1989).
- ³⁹S. Y. Ren, J. D. Dow, and D. J. Wolford, Phys. Rev. B **25**, 7661 (1982).
- ⁴⁰N. Lathiotakis and A. N. Andriotis, Solid State Commun. **87**, 871 (1993).
- ⁴¹R. Scholz, J.-M. Jancu, and F. Bassani, Mat. Res. Soc. Symp. Proc. (to be published).
- ⁴²D. Porezag, T. Frauenheim, T. Köhler, G. Seifert, and R. Kaschner, Phys. Rev. B **51**, 12 947 (1995).
- ⁴³T. Frauenheim, F. Weich, T. Köhler, S. Uhlmann, D. Porezag, and D. Seifert, Phys. Rev. B **52**, 11 492 (1995).
- ⁴⁴U. Schmid, N. E. Christensen, and M. Cardona, Phys. Rev. B **41**, 5919 (1990).
- ⁴⁵D. N. Mirlin, V. F. Sapega, I. Ya. Karlik, and R. Katilius, Solid State Commun. **61**, 799 (1987).